Gain Bandwidth Enhancement and Sidelobe Level Stabilization of mm-Wave Lens Antennas Using AI-driven Optimization

Mwang'amba, Rahabu; Mei, Peng; Akinsolu, Mobayode; Liu, Bo; Zhang, Shuai

Published in:
I E E E Antennas and Wireless Propagation Letters

DOI (link to publication from Publisher):
10.1109/LAWP.2024.3382028

Publication date:
2024

Document Version
Accepted author manuscript, peer reviewed version

Gain Bandwidth Enhancement and Sidelobe Level Stabilization of mm-Wave Lens Antennas Using AI-driven Optimization

Rahabu Mwang'amba, Peng Mei, *Member, IEEE*, Mobayode O. Akinsolu, *Senior Member*, *IEEE*, Bo Liu, *Senior Member*, *IEEE*, and Shuai Zhang, *Senior Member, IEEE*

***Abstract*— This paper explores the transformative potential of artificial intelligence (AI) techniques in optimizing the phase distributions of a lens antenna to significantly enhance the gain bandwidth and stabilize the sidelobe levels at the millimeter-wave band. Through an AI-driven antenna design method (self-adaptive Bayesian neural network surrogate-model-assisted differential evolution for antenna optimization (SB-SADEA), specifically), this work obtains a phase distribution that provides a wide gain bandwidth and stable sidelobe levels from 24 to 33 GHz. A lens antenna with 20 × 20 unit cells is implemented based on the phase distribution. Results show a 1-dB bandwidth of 28.2% and the sidelobe levels have also been lowered compared to the reference design. The optimized lens antenna shows a stable gain with a range of 20.13 dB to 22.16 dB from 24 to 33 GHz, in comparison to the reference design that has a gain range of 16.70 dB to 26.43 dB over the same frequency spectrum. The measured results align well with the simulated results, verifying the effectiveness of the AI-driven antenna design optimization technique in enhancing the performance of a lens antenna.**

***Index Terms* — Directive lens antenna, phase distribution, 1-dB gain bandwidth, sidelobe level, artificial intelligence, SB-SADEA.**

I. INTRODUCTION

With the advent of 5G and beyond networks, antennas are expected to deliver not only high data rates but also low latency and reliable connections in countless scenarios, from densely populated urban centers to remote rural areas. To meet these escalating demands, antennas should be designed to operate over a wide range of frequencies, making bandwidth a crucial performance metric [1], [2]. Lens antennas have gained popularity due to their immense flexibility in their deployment across applications ranging from satellite communication to radar systems and wireless networks. However, a primary challenge associated with metasurface-based lens antennas lies in their inherently narrow-band behavior [3]. As these antennas generally consist of resonant elements, often microscale in nature, their bandwidths are rather limited.

A significant body of research has focused on enhancing the bandwidth of lens antennas [4]-[9]. In [5], a lens antenna was constructed by placing a circularly polarized patch antenna at the focal point of the metasurface with enhanced 6% 1-dB gain bandwidth through varying the rotation angle to compensate for the phase delay. [6] utilizes the drilling of numerous variable square holes to a dielectric host material of the lens antenna technique, to enhance 1-dB gain bandwidth by 13.8%. A simple single-layer metasurface lens with negative refractive index behavior to improve the focusing characteristics of the lens is proposed in [7] to attain a 17% 1-dB gain bandwidth. Moreover, a double-layer metallic pattern etched on both sides Huygens metasurface was designed for meta-lens to enhance the gain bandwidth by ensuring the nearly complete available transmission phase coverage through induced magnetism for Huygen's resonance [8], [9].

Considering all the methods above, techniques involve either adding structures or shapes to improve the 1-dB gain bandwidth which increases design complexity; Hence, their performance might not be optimal. With the growing use of artificial intelligence (AI) techniques in contemporary antenna design, it is possible to deduce optimal design parameters automatically via AI-driven antenna design optimization algorithms, reducing the design complexity and exploring the full potential of antenna structures [10]. Some works have utilized pure evolutionary computation techniques such as genetic algorithms to provide ultra bandwidth at lower frequencies for lens antennas [11].

This paper adds to the body of knowledge by utilizing a machine learning-assisted global optimization method for antenna design to optimize the phase distribution of a lens antenna for 1-dB gain bandwidth enhancement and stable sidelobe levels from 24 to 33 GHz. The motivation is rooted in the necessitated capability of antennas to support the high bandwidth demands of 5G networks, Internet of Things (IoT) devices, and beyond by considering the optimal phase distribution for a lens antenna. The implications of the work are positioning lens antennas as pivotal components in the evolution of wideband communication systems.

II. PROBLEM FORMULATION WITH A LENS ANTENNA

Fig. 1 presents the configuration of the lens antenna, which

Manuscript received Feb. 2024. *(Corresponding author: Peng Mei)*

R. Mwang'amba, P. Mei, and S. Zhang are all with the Antennas, Propagation and Millimeter-wave Systems (APMS) section, Department of Electronic Systems, Aalborg University, Aalborg, 9220, Denmark. (Email: rahabum@es.aau.dk, mei@es.aau.dk, sz@es.aau.dk)

M. O. Akinsolu is with the Faculty of Arts, Computing, and Engineering, Wrexham University, Wrexham, U.K. (Email: m.o.akinsolu@ieee.org)

B. Liu is with the James Watt School of Engineering, University of Glasgow, Glasgow, Scotland, U.K. (Email: bo.liu@glasgow.ac.uk)

consists of a feed source and a lens metasurface. The lens metasurface is properly configured to convert the spherical waves from the feed source to the plane waves for a high gain. It should be noted here that the performance of the lens antenna is closely related to the spatial relation between the lens metasurface and feed source as well as the phase compensations of the lens metasurface. Generally, the phase of each unit cell of the lens metasurface should be provided and calculated according to Eq. (1):

$$\theta_i(x_i, y_i, z_i) = -2\pi/\lambda \cdot \sqrt{(x_s - x_i)^2 + (y_s - y_i)^2 + (z_s - z_i)^2} \quad (1)$$

where (x_i, y_i, z_i) is the location of the unit cell i, (x_s, y_s, z_s) is the phase center of the feed source and λ is the wavelength of interest. Eq. (1) is frequency-dependent, which potentially limits the gain bandwidth of the corresponding lens antenna.

To increase the bandwidth and augment other performance (i.e., stable sidelobe levels within a wide bandwidth) of a lens antenna, an efficient method of AI-driven optimization is proposed here and elaborated in Section III. By properly defining the objective functions, the proposed optimization scheme can achieve gain enhancement and stable sidelobe levels within a wide bandwidth by simultaneously optimizing the amplitude and phase distributions of a lens antenna.

The verification of the proposed method is done by configuring the lens metasurface with and without the proposed optimization scheme, where the latter is used as the reference design. For brevity, the unit cell with a periodicity of W to build the lens metasurface is based on a dielectric rod (depicted in Fig. 1(b)) that has been widely adopted to implement lens antenna in the literature. Here, acrylonitrile butadiene styrene (ABS) with a relative permittivity of 2.55, a relative permeability of 1, and a loss tangent of 0.01 was selected because this material has a combined effect of heat resistance and low capability of being affected by galvanic corrosion. Air voids are drilled into the bottom and top layer to improve transmission efficiency of the unit cell. A full phase-cycle coverage (2π) is achieved by tuning the height of the unit cell (h_i) from 5.13 mm to 24.97 mm. The planar lens metasurface composed of 20 × 20 unit cells was initially positioned at a distance d = 42 mm from the feed source (horn antenna) and was illuminated by spherical waves radiated from the feed source.

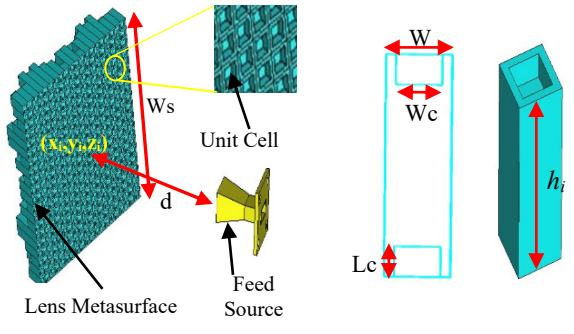

Fig. 1. a) Implementation of the lens antenna and its simulation setup. b) Unit cell structure. (Ws = 100 mm, W = 5 mm, Wc = 3.5 mm, Lc = 2.5 mm)

III. AI-Driven Optimization Using SB-SADEA

The lens antenna with 20 × 20 unit cells presented in this work presents an atypical antenna design optimization problem. This stems from the number of critical design parameters that influence its frequency responses and the performance specifications that it must fulfill to make it suitable for the desired mm-Wave application (see Tables I and II). With 101 critical design parameters (due to the high symmetrical structure of the lens antenna, the total 401 critical design parameters ($20\times20 + d$) is reduced to 101) and 70 performance specifications as reported in Table I and Table II, respectively, the optimization of the amplitude and phase distributions of the lens antenna is exceedingly difficult by manual optimization. Off-the-shelf optimization techniques, such as genetic algorithms, are also difficult to use because several tens of thousands of electromagnetic (EM) simulations are needed, costing prohibitive time. Hence, self-adaptive Bayesian neural network surrogate model-assisted differential evolution for antenna optimization (SB-SADEA), a purpose-built method for the machine-learning-assisted global optimization of high-dimensional antenna structures [12] is employed.

TABLE I: SEARCH RANGES OF THE DESIGN PARAMETERS AND THE OPTIMAL DESIGN BY SB-SADEA FOR THE LENS ANTENNA (ALL DIMENSIONS ARE IN mm)

Design Variables	Lower Bound	Upper Bound	SB-SADEA-Optimized Design Lens Metasurface Geometry
$h_{j\in[1,2,\ldots,100]}$	5.00	25.00	h_{opt}
d	40.00	120.00	40.43

Where:
h_{opt} = [14.69,14.79,14.61,24.63,20.96,24.11,18.53,15.55,6.34,17.95,13.24, …
22.40,16.30,19.97,18.08,18.05,15.61,22.72,12.64,9.68,11.73,8.99, …
14.69,7.71,10.59,7.12,7.14,8.73,5.13,16.02,12.23,10.35,20.62,13.59…
8.90,8.82,5.52,7.06,12.06,24.05,16.61,14.18,8.22,10.32,15.73,7.38, …
11.41,2027,17.89,23.93,22.73,6.53,22.95,14.12,6.81,15.89,18.31, …
18.24,18.87,9.66,21.80,5.71,11.79,9.24,17.43,11.49,21.85,20.04, …
22.80,17.23,21.16,17.25,14.10,15.63,5.74,21.78,11.18,24.97,18.60, …
8.29,20.89,21.23,7.67,7.73,14.00,22.79,22.59,23.95,24.70,14.85, …
8.74,12.58,9.61,17.77,19.27,16.36,23.20,21.94,24.29]

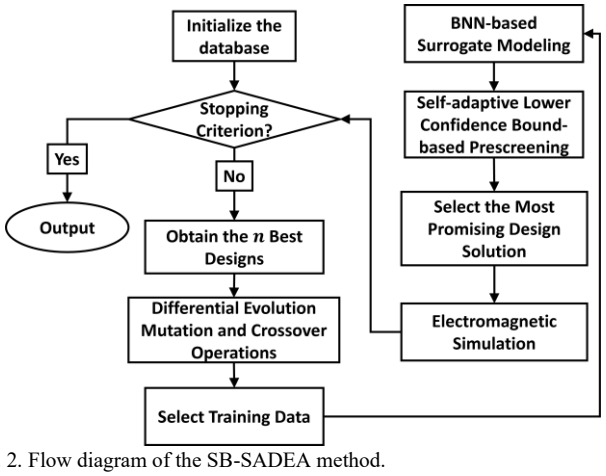

Fig. 2. Flow diagram of the SB-SADEA method.

The essential steps in the SB-SADEA workflow are shown in Fig. 2 and discussed as follows for the targeted antenna, and additional information about the SB-SADEA method is available in [12]:

1) *Step 1:* Initialization by sampling the lens antenna's design

space and the execution of full-wave EM simulations. According to [12], 4×d (d is the number of design variables) candidate designs generated using the Latin hypercube sampling method [13] are used to form the initial database. SB-SADEA is an online machine learning-assisted global optimization technique, for which, the surrogate model keeps updating in the optimization process. Hence, the number of the initial samples is small [12],[14].

2) *Step 2:* Creation of the initial database comprising the sample designs from Step 1 and their simulation results.

3) *Step 3:* Extraction of the current population, which is composed of the current top n optimal candidate designs (i.e., the candidate designs with the top n objective function values) from the database. If the computing budget is exhausted, output the current best design and terminate.

4) *Step 4:* Creation of new offspring solutions via differential evolution (DE) mutation and crossover operations, which are applied to the population in *Step 3*.

5) *Step 5:* Obtaining samples from each offspring solution that is closest (based on the Euclidean distance) to use as training data points, and the construction of a surrogate model based on a Bayesian neural network (BNN) [12]. The BNN model is used for predicting the performance of candidate designs in *Step 4*.

6) *Step 6:* Self-adaptive lower confidence bound-based prescreening of the offspring solutions using the predicted performance and prediction uncertainty from *Step 5* [12].

7) *Step 7:* Selection and simulation of the predicted best offspring solution and adding the solution and its simulation results to the database. Go back to *Step 3*.

For the SB-SADEA-driven optimization of the lens antenna, the design parameters described in Fig. 2 and their search ranges in Table I have been considered. A population size of 410 is used and all other algorithmic parameters have the default settings in [12]. The optimization goal is to make the specifications listed in Table II better than those of the reference design through the minimization of the fitness function P. Specifically, for specifications (1) to (7) in Table II, the thresholds to surpass are their values derived from the performance of the reference design, and for specifications (8) to (10) in Table II, the goal is to have the sum of the mean absolute deviations of the simulated gains to be close to zero (as much as possible) to ensure a smooth and ripple-free descent of the gain pattern from θ =0° to θ =14^0. It should be noted that the selection of θ =14^0 is a compromise for examining the radiation patterns of the reference lens antenna at different frequencies, and different θ may lead to distinct computations in the AI-driven design optimization process.

$$Freq. = \left[24GHz, 25GHz, 26GHz, 27GHz, 28GHz, 29GHz, 30GHz\right] \quad (2)$$

For (θ =0 °and ϕ=0°):

$$P_1 = w_1 \times \left\{ \sum_{k \in Freq.}^{\forall k} \max\left(\left[G^k_{bore\_ref} - G^k_{bore}, 0 \right] \right) \right\} \quad (3)$$

For

$$Ang1. = [(\theta = [0° \text{ to } 14°] \text{ and } \phi = 0°), (\theta = [0° \text{ to } 14°] \text{ and } \phi = 45°), (\theta = [0° \text{ to } 14°] \text{ and } \phi = 90°)] \quad (4)$$

$$P_2 = \sum_{\forall Cond1. \in Ang1.}^{\forall Cond1.} \left\{ w_1 \times \left\{ \sum_{k \in Freq.}^{\forall k} \max\left(\left[G^k_{norm_{ref}} - G^k_{norm}, 0 \right] \right) \right\} \right\} \quad (5)$$

$$P_3 = \sum_{\forall Cond1. \in Ang1.}^{\forall Cond1.} \left\{ w_2 \times \left\{ \sum_{k \in Freq.}^{\forall k} abs\left(\left[G^{k_{m+1}}_{simulated} - G^{k_m}_{simulated} \right] \right) \right\} \right\} \quad (6)$$

For

$$Ang2. = [(\theta = [>14° \text{ to } 180°] \text{ and } \phi = 0°), (\theta = [>14° \text{ to } 180°] \text{ and } \phi = 45°), (\theta = [>14° \text{ to } 180°] \text{ and } \phi = 90°)] \quad (7)$$

$$P_4 = \sum_{\forall Cond2. \in Ang2.}^{\forall Cond2.} \left\{ w_1 \times \left\{ \sum_{k \in Freq.}^{\forall k} \max\left(\left[G^k_{norm} - G^k_{norm\_ref}, 0 \right] \right) \right\} \right\} \quad (8)$$

$$P = P_1 + P_3 + P_2 + P_4 \quad (9)$$

where k_m is the m-th element in $Freq.$, k_{m+1} is the next element after the m-th element in the same set, and w_1=500 and w_2=5000 are used to allow the optimization process preferentially ensure that the gain patterns for each simulated frequency (i.e., k) considered are smooth and ripple-free in their descent from θ =0° to θ =14°, before focusing on making the boresight gain and side-lobe levels better than those of the reference design.

TABLE II
PERFORMANCE SPECIFICATIONS (FREQUENCIES: 24 GHz, 25 GHz, 26 GHz, 27 GHz, 28 GHz, 29 GHz, and 30 GHz)

Item	Specification corresponding to each frequency
1.	Boresight gain ($G^{k\in[24GHz,25GHz,...,30GHz]}_{bore}$) (θ = 0^0 and ϕ = 0^0)
2.	Minimum normalized gain ($G^{k\in[24GHz,25GHz,...,30GHz]}_{norm}$) (θ = [0^0 to 14^0] and ϕ = 0^0)
3.	Minimum normalized gain ($G^{k\in[24GHz,25GHz,...,30GHz]}_{norm}$) (θ = [0^0 to 14^0] and ϕ = 45^0)
4.	Minimum normalized gain ($G^{k\in[24GHz,25GHz,...,30GHz]}_{norm}$) (θ = [0^0 to 14^0] and ϕ = 90^0)
5.	Maximum normalized gain ($G^{k\in[24GHz,25GHz,...,30GHz]}_{norm}$) (θ = [> 14^0 to 180°] and ϕ = 0^0)
6.	Maximum normalized gain ($G^{k\in[24GHz,25GHz,...,30GHz]}_{norm}$) (θ = [> 14^0 to 180°] and ϕ = 45^0)
7.	Maximum normalized gain ($G^{k\in[24GHz,25GHz,...,30GHz]}_{norm}$) (θ = [> 14^0 to 180°] and ϕ = 90^0)
8.	Sum of the absolute deviation of the simulated gain ($G^{k\in[24GHz,25GHz,...,30GHz]}_{simulated}$) (θ = [0^0 to 14^0] and ϕ = 0^0)
9.	Sum of the absolute deviation of the simulated gain ($G^{k\in[24GHz,25GHz,...,30GHz]}_{simulated}$) (θ = [0^0 to 14^0] and ϕ = 45^0)
10.	Sum of the absolute deviation of the simulated gain ($G^{k\in[24GHz,25GHz,...,30GHz]}_{simulated}$) (θ = [0^0 to 14^0] and ϕ = 90^0)

Note:
Items (1) to (7) constitute a total of 49 specifications (i.e., seven specifications for each frequency considered).
Items (8) to (10) constitute a total of 21 specifications (i.e., seven specifications for each frequency considered).

Overall, the lens antenna has been modeled and discretized in the Computer Simulation Technology – Studio Suite using a mesh density of 15 cells per wavelength to have about 5, 500, 000 hexahedral mesh cells in total. It is then analyzed using the finite integration technique with a time-domain solver having

an accuracy of -40 dB. Each EM simulation costs about 10 minutes on average (from a wall clock) on a workstation with Intel 6-core i9-990K 3.60 GHz CPU and 64.0 GB RAM. After 3,880 EM simulations, SB-SADEA obtained a satisfactory design with P = 1.16e+04. This design is reported in Table I and its characterization and physical implementation are discussed in the subsequent sections.

IV. Simulation and Measurement

According to the optimized heights of all the unit cells listed in Table. I, the phase distribution on the lens metasurface is therefore plotted as illustrated in Fig. 3 (a). To demonstrate the improved performance of the optimized lens metasurface, the phase distribution of the reference lens antenna is shown in Fig. 3(b), where the phase distribution is calculated with Eq. (1) at 28 GHz with d = 40. 43 mm. Then, both lens metasurfaces are implemented with the unit cells illustrated in Fig. 1(b), and their performance is simulated and compared.

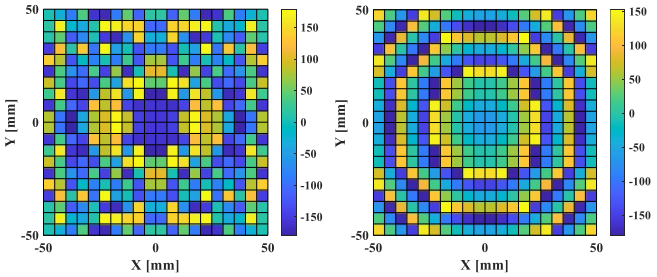

Fig. 3. Phase distributions at 28 GHz. (a). Optimized lens antenna. (b). Reference lens antenna.

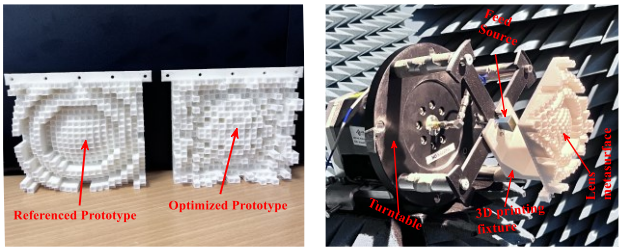

Fig. 4. (a) Reference and optimized prototypes (b) Experimental setup

Prototypes of the optimized and reference lens antennas were manufactured using 3D printing technology and were also measured in the anechoic chamber. To align the distance between the feed horn and the lens, a fixture is also printed to permit the distance as illustrated in Fig. 4. Although the optimization band in Section III is from 24 to 30 GHz, we measure 24 to 33 GHz to check the gains and sidelobe levels to demonstrate the robust of the optimization. From Fig. 5(a), it is seen that the measured and simulated realized gains of the reference lens antenna range from 16.70 dB to 26.43 dB and 17.50 dB to 26.32 dB from 24 GHz to 33 GHz, respectively. In contrast, the optimized lens antenna realizes low gain fluctuation with its peaks observed to be 22.37 dB and 22.15 dB for simulated and measured results respectively with their range difference around 2 dB for the chosen frequency range. In addition to wide gain bandwidth, stable sidelobe levels in the optimized design are observed, which is illustrated in Fig. 5(b). While SLLs range from -17.18 dB to -20.05 dB and -16.70 dB to -20.80 dB for measured and simulated optimized designs, respectively. In contrast, the reference design SLLs' fluctuation is higher than 10 dB for the entire frequency band, with their peaks at -9.98 dB and -11.0 dB for measured and simulated results, respectively. The comparison is also done by considering the radiation patterns at different operating frequencies as shown in Fig. 6. The measured results are consistent with the simulated results. The little discrepancy can be ascribed to fabrication and measurement tolerances.

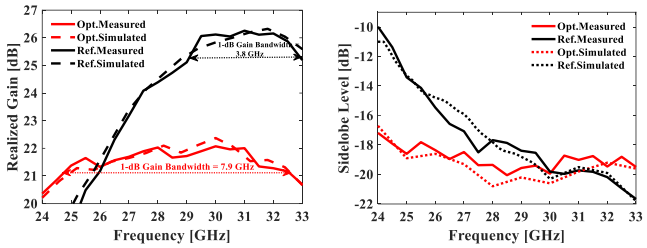

Fig. 5. Comparison of simulated and measured results of the reference and optimized lens antennas. (a) Realized gain from 24 GHz to 33 GHz. (b). sidelobe levels from 24 GHz to 33 GHz.

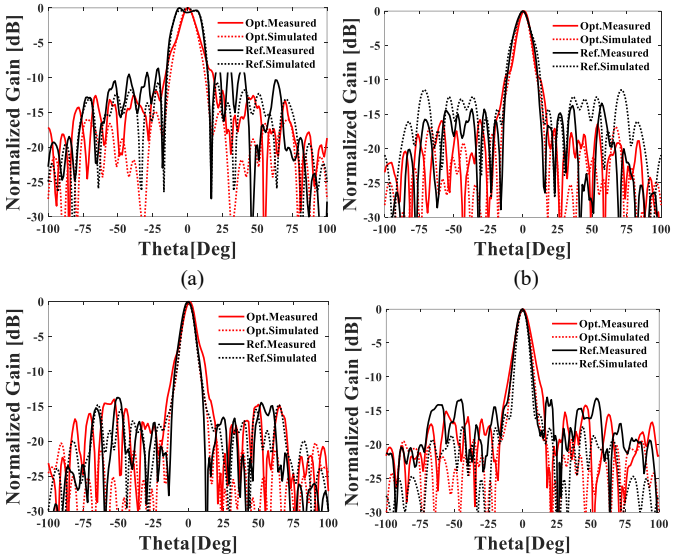

Fig. 6. Comparison of gain pattern between measured and simulated results at different operating frequencies (a) 24 GHz (b) 26 GHz (c) 28 GHz (d) 30 GHz

V. Conclusion

In summary, this work has presented the use of AI-driven antenna design techniques (particularly, the SB-SADEA method) to optimize the phase distribution of a lens antenna to attain a wide 1-dB gain bandwidth and stable sidelobe levels. Measurements show a 1-dB gain bandwidth of 28.2% and stable sidelobe levels around -18 dB from 24 to 33 GHz for the optimized lens antenna. The results of this work are important in modern communication systems as they offer a transformative approach by utilizing artificial intelligence to overcome narrowband limitations and harness the full potential of lens antennas for wideband applications.

REFERENCES

[1] H. Giddens, and Y. Hao, "Multibeam graded dielectric lens antenna from multimaterial 3-D printing," *IEEE Trans. Antennas Propag*., vol. 8, no. 9, pp. 6832–6837, Sep. 2020.

[2] R. A. dos Santos, G. Lobão da Silva Fré, L. G. da Silva, M. C. de Paiva, and D. H. Spadoti, "Ultra-wideband dielectric lens antennas for beam steering systems," *Int. J. Antennas Propag*., vol. 2019, p. e6732758, Aug. 2019.

[3] D. Sievenpiper, L. J. Zhang, R. F. J. Broas, N. G. Alexopolous, and E. Yablonovitch, "High-impedance electromagnetic surfaces with a forbidden frequency band," *IEEE Trans. Microw. Theory Tech*., vol. 47, no. 11, pp. 2059–2074, Nov. 1999.

[4] M. Karimipour, M. B. Heydari, and I. Aryanian, "Broadband high-efficiency 3-bit coding metasurface in transmission mode based on the polarization conversion technique," *Sci. Rep*., vol. 13, no. 1, Art. no. 1, Jul. 2023.

[5] Y. Zhuang, G. Wang, H. Li, and W. Guo, "Novel high-gain circularly polarized lens antenna using single-layer transmissive metasurface," *Frequenz*, vol. 71, no. 5–6, pp. 267–272, Mar. 2017.

[6] S. L. Liu, X. Q. Lin, J. Y. Lan, and X. B. He, "W-band flat lens antenna with compact size and broadband performance," *IET Microw. Antennas Propag*., vol. 14, no. 10, pp. 1047–1052, 2020.

[7] C. M. Saleh, E. Almajali, A. Jarndal, J. Yousaf, S. S. Alja'Afreh, and R. E. Amaya, "Wideband 5G antenna gain enhancement using a compact single-layer millimeter wave metamaterial lens," *IEEE Access*, vol. 11, pp. 14928–14942, 2023.

[8] S. Cao, J. Zhou, R. Li, and C. Xue, "A double-layer dual-polarized Huygens metasurface and Its meta-lens antenna applications," *Micromachines*, vol. 14, p. 1139, May 2023.

[9] J. Zhou, Y. Xiong, Q. Peng, Z. Bin, and C. Xue, "A double-layer Huygens' metasurface with complete phase coverage and its dual-polarized meta-lens antenna application," *Front. Phys*., vol. 11, Sep. 2023.

[10] W. Dou *et al*., "Antenna artificial intelligence: the relentless pursuit of intelligent antenna design [Industry Activities]," *IEEE Antennas and Propagation Magazine*, vol. 64, no. 5, pp. 128-130, Oct. 2022.

[11] W. S. Yu *et al*., "An ultrawideband and high-aperture-efficiency all-dielectric lens antenna," *IEEE Antennas Wireless Propag Letts*, vol. 20, no. 12, pp. 2442-2446, Dec. 2021.

[12] Y. Liu *et al*., "An efficient method for antenna design based on a self-adaptive Bayesian neural network-assisted global optimization technique," *IEEE Trans. Antennas Propag.*, vol. 70, no. 12, pp. 11375-11388, Dec. 2022.

[13] M. Stein, "Large Sample Properties of Simulations Using Latin Hypercube Sampling," *Technometrics*, vol. 29, no. 2, pp. 143-151, May 1987.

[14] B. Liu et al., "An efficient method for antenna design optimization based on evolutionary computation and machine learning techniques." *IEEE Trans. Antennas Propag*., vol 62, no. 12, pp. 7-18. Jan. 2014.